ANODE WIRE SWELLING – A NEW PHENOMENON IN ANODE WIRE AGING UNDER HIGH-ACCUMUPATED DOSE

G.E.Gavrilov, A.I.Egorov, A.G.Krivchitch, E.N.Kuznetsova, V.M.Lebedev, L.A.Schipunov

1. Introduction

High-energy physics detectors proposed for the Large Hadron Collider (LHC) demand a higher performance than is available from conventional gas detectors [1]. These detectors are intended to operate without a service access for several years. The radiation level near the beam of a storage ring collider can result in an integrated charge level of 10–13 C/cm after about 10 years of operation. This is at least an order of magnitude more than what has been achieved in previous experiments. It is clear that the next generation of wire chambers will need higher levels of radiation hardness. Thus, the study of aging effects for these new detectors is important and timely.

Usually, aging effects result in a surface degradation of both the anode and cathode electrodes, which occurs in the form of "deposits" [2]. These deposits are generally some form of polymer or, in certain cases, may be elemental carbon. Another type of wire (or cathode) surface degradation is a chemical attack on the wire surface by an active species produced in the gas avalanche. This may occur for non-gold plated wires which contain chemically active elements in the wire surface material [3]. The explanations for both of these mechanisms can be addressed in terms of plasma chemistry. Different types of chemical radicals and ions produced in the gas avalanche near the anode wire may cause plasma chemical reactions. Polymers resulting from the reactions of the radicals may deposit upon and coat the surface of the chamber electrodes, and even create new chemically different substances after interacting with the electrode materials.

Some time ago, a new aging mechanism of the anode wire – the swelling of the wire under high-accumulated dose – was observed for the first time [1]. It was a new, unexpected process causing the deterioration of gas detectors. The principal difference between the anode wire-swelling phenomenon and the well-known polymerization mechanism of aging is that the forces are applied from <u>within the wire</u> breaking the gold coating. As a result of this process, the wire diameter increases (see section 3). Also, an intense concentration of oxygen has been observed on the open tungsten surface.

We surmise that the anode-swelling phenomenon is quite complicated and needs more investigation. That is why we are trying to describe just the general items of the phenomenon and have no pretensions that this process is entirely understood. Our goal is to show the interconnection between the main factors causing both the anode wire swelling and the development of aging.

We would like to point out the main goals of this article. The first is the presentation of the experimental data which confirm the phenomenon of a new aging mechanism and show that oxygen plays very important role in the wire aging process under a high-accumulated dose. Second, we propose a hypothesis that the tungsten oxidation process can explain anode wire swelling. So, now we are just talking about anode swelling as a phenomenon, which is interesting itself and could be interesting for physicists investigating wire aging both at real experiment conditions and for the design of gas-filled detectors. That is why many of these questions, which are important in the every-day practice of an experimenalist, are appropriate for a following more careful study.

2. Aging results

2.1. Test setup

The data were obtained during aging tests of straw tubes with a 70%Xe + 10%CO_2 + 20%CF_4 working gas mixture. The aging studies were performed at PNPI (Gatchina) using the Aging Test Station (ATS) [2].

---

[1] ATLAS Technical design report, Inner Detector, ATLAS TDT 5, CERN/LHCC 97-17.
[2] J.A.Kadyk, Nucl. Instr. Meth. **A300**, 436 (1991).
[3] M.Atas, IEEE Trans. Nucl. Sci. **NS-34**, 476 (1987); J.A.Kadyk, IEEE Trans. Nucl. Sci. **NS-43**, 481 (1987).

The degradation test of the detector was carried out using a ^{90}Sr β-source of two-Curie radioactivity. The width of the beam is about FWHM = 1.5 cm. The profile of the irradiated zone was confirmed by exposing a photographic film positioned in the place of the wire. Two straw tubes [4] used in our investigations had diameters of 4 mm and length of 32 cm. The cathode consisted of a 50 μm carbon coated Kapton film, and the anode wire was made of gold-coated tungsten with a diameter of 35 μm. The supplier ("Mashinistroitel" Company, Saratov, Russia) specified the gold thickness to be 1.1 μm. During the test, a premixed gas mixture was transported *via* 6 m long stainless steel line connected to the straws. The gas flow rate was 0.2 cm^3/min, which corresponds to two straw volumes per hour.

Measurements of the straw tube properties were made regularly every few days during the exposure. When the ^{90}Sr source was removed, the dark current was recorded. To monitor the gas gain, the peak position of the pulse-height distribution from the ^{55}Fe source was measured. In order to be as close as possible to the real experimental conditions, the applied high voltage was chosen so as to compensate for the space charge effect that decreases the gas gain under intense irradiation and keep the gas gain in the center of irradiation zone at 3×10^4. At this gas gain, the straw tube had a rate of charge accumulation of 0.15 C/cm per day.

2.2. Results of SEM/XEM analysis

The analysis of the anode surface after aging was performed using a scanning electron microscope with *X*-ray emission (0–10 keV) spectroscopy (SEM/XEM). The SEM/XEM analysis yielded information on the morphology of the wire surface, by imaging the scattered and secondary electrons, and on the atomic composition of a very thin surface layer by *X*-ray fluorescence spectroscopy. The quantitative evaluation of the element content in the depth of the material is practically impossible because of the strong *X*-ray absorption by the wire material.

The results of the SEM/XEM analysis obtained from different points on the wire are presented in Fig. 1. Measurements were carried out both in the centre of the irradiated zone (X = 0 cm) and at the edge of the wire (X = −14 cm) very far from the irradiated zone. As one can see, the wire surface in the non-irradiated zone is smooth and undamaged and the XEM measurement indicates only a gold surface. In the centre of the irradiated zone, the gold coating is broken and the wire diameter has increased by 20% (from 35 up 42 μm) at an accumulated charge of Q = 9 C/cm.

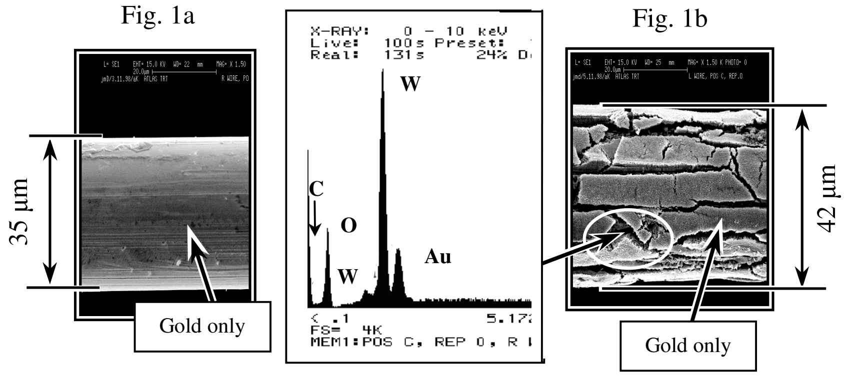

Fig. 1. Anode wire swelling effect. The scale (20 μm length) is indicated as a white line in the top part of both Figs. 1a, 1b. The arrow indicates the location of possible carbon content. Results of SEM examination of the wire surface in the non-irradiated zone and in the centre of irradiation are presented in Figs. 1a, 1b

SEM/XEM analysis of the surface of the wire gold coating showed only the presence of gold. Any visible traces of other elements (*e.g.* fluorine and carbon) that could be coming from the avalanche plasma were not observed either on the gold coating or on the tungsten surface. However, the opened tungsten surface contained an intense oxygen peak among the pieces of gold coating.

We did not observe any noticeable amount of polymer deposits on the surface of the gold coating of the wire. This means that we cannot explain the increase of the wire diameter in the usual way.

[4] T.Akesson *et al.*, Nucl. Instr. Meth. **A367**, 143 (1995).

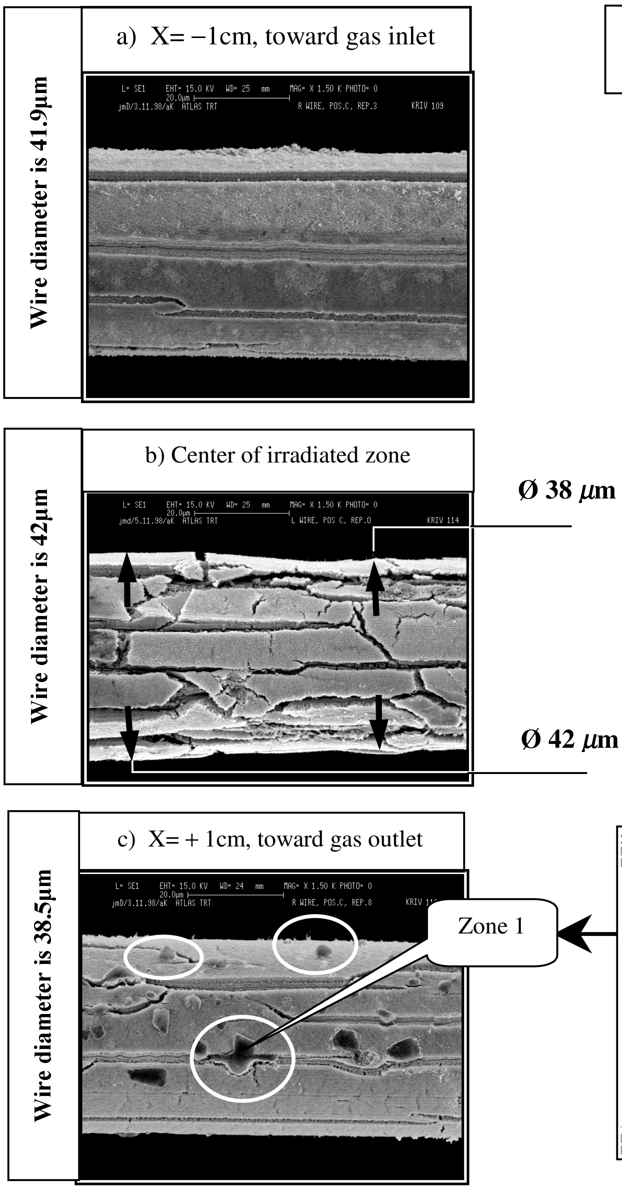

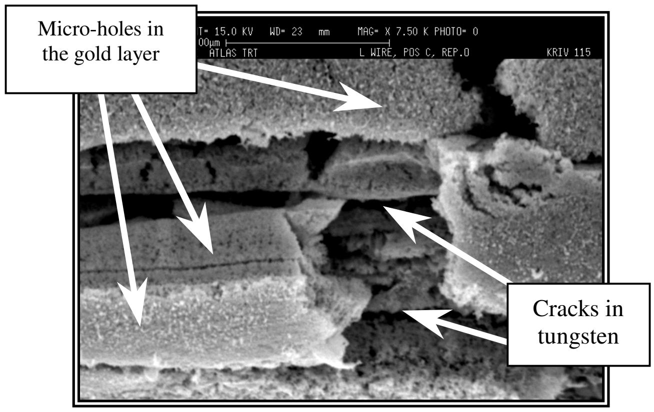

Fig. 3. SEM micrograph of the anode wire surface in the center of the irradiated zone. The scale (5 μm length) is indicated by the white line on the top part of the picture. The diameter of the micro-holes is less than 0.2 μm

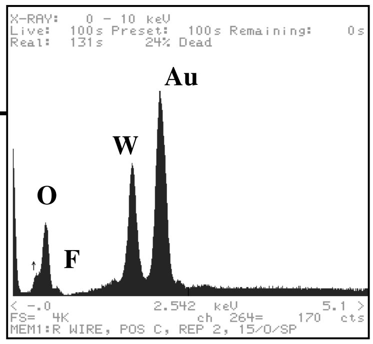

Fig. 2. Results of SEM/XEM examination of the anode wire surface in the centre of the irradiated zone and ± 1cm to each side – see Figs. 2a,b,c. Tungsten and oxygen were detected in the white rings (for instance, Zone 1) in the gold layer. The scale (20 μm) is indicated by a white line in the top part of all figures

Fig. 2d. Results of XEM spectra analysis of the deposits measured in Zone 1 (Fig. 2c) are presented here. Similar spectra containing tungsten and oxygen were observed at different points along the wire outside of the irradiated zone

Thus, we propose that under the intense irradiation regime (about 1.7 μA/cm and a dose of 9 C/cm per wire) a new aging mechanism occurs for anode wires – the swelling of the wire, leading to surface damage [1].

The results of the SEM/XEM examination of the anode wire surface, both inside and outside of the irradiation zone, are presented in Figs.1–4. As one can see, in the irradiation zone $|X| \leq 1$ cm the gold coating is broken and the wire diameter has swollen to a maximum value of 42 μm in the centre of the irradiation zone (X = 0 cm). The gold layer, as a result of irradiation, has become quite porous, as one can see in Fig. 3 where a SEM micrograph of the irradiated anode wire surface is shown. The wire diameter decreases to the original wire diameter of 35 μm outside of the irradiated zone (see Fig. 4).

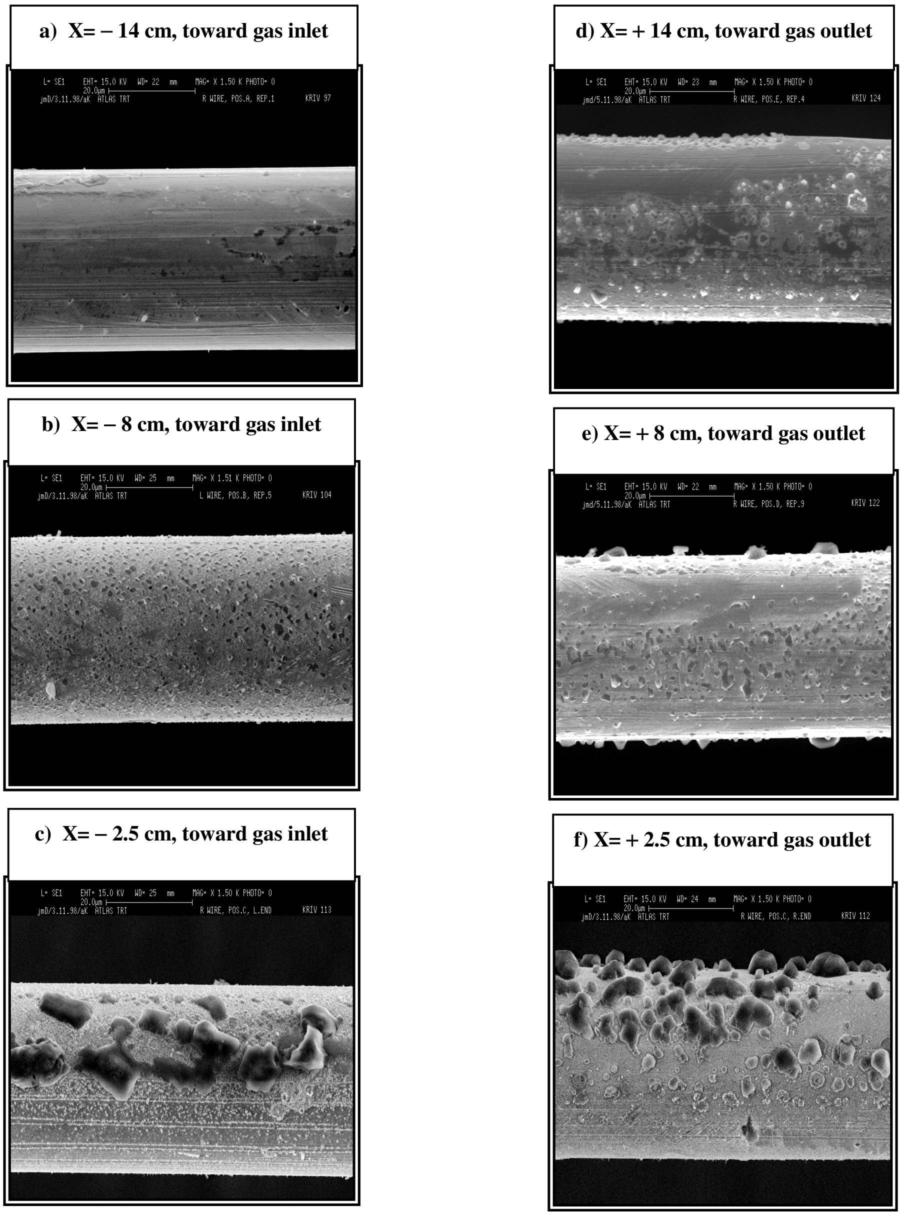

Fig. 4. Results of SEM/XEM examination of the anode wire surface outside of the irradiated zone – $|X| \geq 2.5$ cm. The diameter of all wires shown above is 35.0 μm. The centre of the local system of coordinates is placed at the centre of the irradiated zone (Fig. 1)

Some deposits on the wire surface have been observed, but only outside of the irradiated zone. The concentration of deposits is distributed along the wire, but asymmetrically with respect to the gas flow direction: the concentration is highest at the gas outlet side of the straw tube. Hence, it can be supposed that radicals and polymers were produced in the irradiated zone and then spread along the wire with the gas flow resulting in deposits on the wire. The presence of some deposits close to the gas inlet is a result of the diffusion of radicals from the irradiated zone in both directions along the straw tubes. This is easy to understand given the slow gas flow rate of just 0.2 cm^3/min (or a velocity of 1.6 cm/min). The XEM spectra obtained from different points along the wire show that the deposits outside the irradiated zone contain intense peaks of tungsten and oxygen and some traces of fluorine. Since the only source of tungsten in the straw tube is the wire material, we assume the following mechanism: atomic oxygen and active radicals spread along the wire with the gas flow, penetrate through imperfections in the gold coating, and then react with the tungsten. The resulting compounds then go out of the gold. Exactly how this latter process happens is still unknown and more study is needed.

2.3. Results obtained by the Nuclear Reaction Analysis

The SEM/XEM analysis is useful for the investigation of surface deposits. However, in order to provide a quantitative evaluation of the distribution of the light elements into the depth of the gold coating of the wires, a Nuclear Reaction Analysis (NRA) was applied [5]. For the detection and quantitative evaluation of the oxygen, carbon and nitrogen content as a function of depth in the gold, the following nuclear reactions with deuterons and protons in the energy range of 0.7−1.1 MeV [3] have been applied:

$^{12}C + d \rightarrow {}^{13}C + p + 2.722$ MeV,

$^{16}O + d \rightarrow {}^{17}O + p + 1.049$ MeV,

$^{14}N + d \rightarrow {}^{15}N + p + 1.305$ MeV.

These investigations were carried out at PNPI at an electrostatic accelerator with a maximum energy of 1.6 MeV. A scheme of the experimental setup is presented in Fig. 5. A deuteron beam of 0.9 MeV was used to analyze the oxygen distribution as a function of depth, and of 1 MeV for the carbon, since the differential cross sections of the nuclear reactions have a plateau at these energies. The nuclear reaction products were detected by a surface-barrier silicon detector at an angle of 135° to the beam axis. The acceptance area of the detector is 1.5 cm^2. To minimize the background due to scattered deuterons, the detector was shielded by an aluminum foil with a thickness of 11 μm (3 mg/cm^2). The diameter of the beam spot on the wire was about 4 mm. The energy resolution of the spectrometer was $\Delta E \sim 70$ keV for $E_\alpha = 5.5$ MeV. The beam current through the wire was 3−5 nA. The depth profile is evaluated directly from an energy spectrum of the emitted particles at a constant beam energy. In this method an emitted energy gives information on a depth where the reaction occurs. The number of secondary protons gives an element content for that depth.

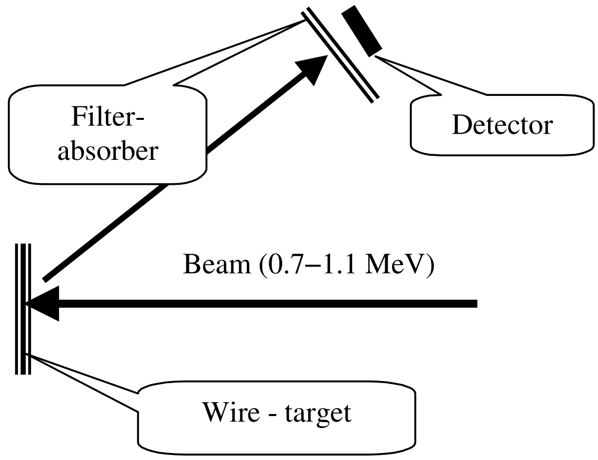

Fig. 5. Schematic representation of the experimental set-up used in the NRA

The results obtained are presented in Figs. 6, 7 for different points along the wire. As one can see from the energy distribution of the protons, the gold coating of the non-irradiated wire contains some oxygen, nitrogen and carbon. After irradiation of the wire, the amount of oxygen and carbon is noticeably increased. It can be seen that the peaks rise and broaden into the low energy region. We conclude that oxygen and carbon have penetrated inside the gold coating of the wire. Taking into account the cross sections of the $^{12}C(d,p)^{13}C$ and $^{16}O(d,p)^{17}O$ reactions [5], the concentration of oxygen inside the gold coating is more than 10 times higher than that of carbon. Because of this result, we consider oxygen to play the most important role in the wire swelling processes, and for this reason only the oxygen data will be analyzed in the rest of this article. The depth distribution of the oxygen concentration inside the wire can be estimated (Fig. 6) from the analysis of the proton spectrum from the (p, d) reaction (Fig. 7). As shown in Fig. 6, with the increase of accumulated dose the oxygen penetrates deeper into the gold layer and the total amount strongly increases.

One can see that even <u>the non-irradiated area</u> of the wire contains oxygen which has already penetrated from the wire surface into the depth of the gold layer up to 1 mg/cm^2 (0.52 μm depth). Similar measurements were taken for clean wires before their installation into the straw tubes. The average concentration of oxygen after the wire manufacturing and at the beginning of the irradiation was about 1×10^{21} at/cm^3.

[5] J.W.Mayer and E.Rimini, *Ion Beam Handbook for Material Analysis*, New York, Academic Press, 1977, p. 488.

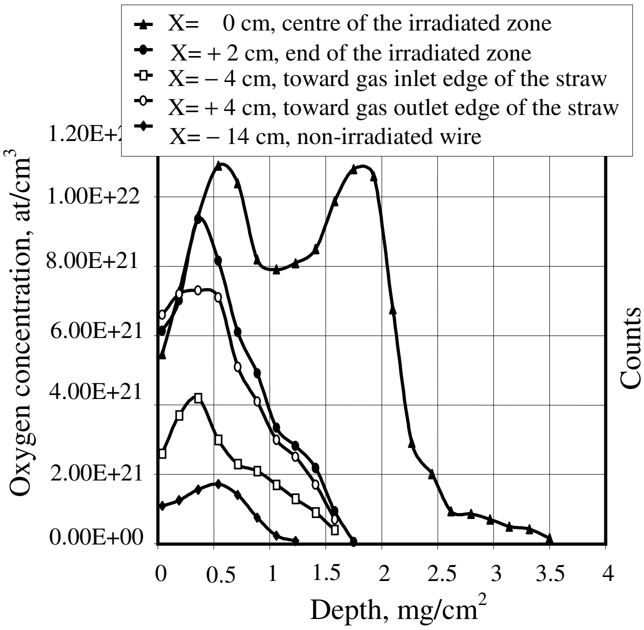

Fig. 6. The distribution of oxygen concentration as a function of depth into the gold layer for different points along the wire

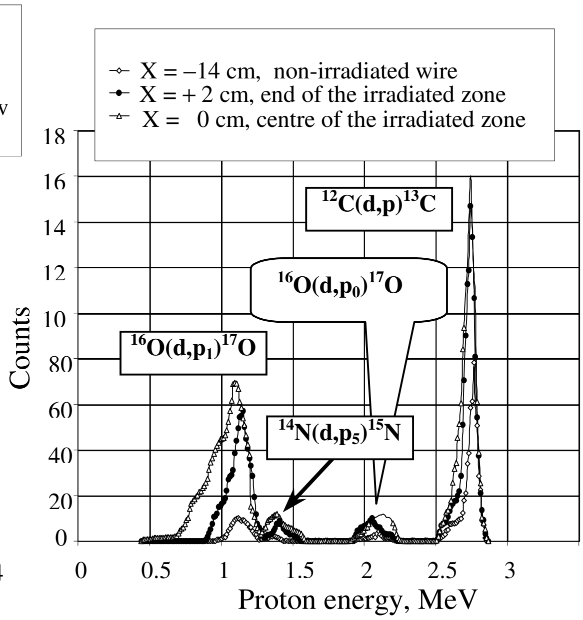

Fig. 7. Proton spectrum from (d, p) reactions on the wire target

The depth distribution of oxygen measured in the vicinity of the edges of the irradiated zone (X= +2 cm) has one peak and contains much more oxygen than in the non-irradiated area. As seen in Fig. 6, with the increase of the accumulated dose (qualitative evaluation is about 2–3 C/cm) the depth of oxygen penetration also increased and achieved a value up to 1.75 mg/cm^2 (about 0.9 μm depth). But this depth is still less than the gold coating thickness (1.2 μm).

The depth distribution of the oxygen concentration in the centre of irradiated zone (X = 0 cm) has a double peak structure that quickly falls at 2.1 mg/cm^2. It is difficult to evaluate precisely the depth (in μm) of the oxygen penetration both in the gold and tungsten because of the damages and the presence of micro-cracks, which can be seen in Figs. 1b and 3, and which reduces the average density of each material. Visual inspection of the gold surface, shown in Fig. 1b, leads us to the conclusion that the cracks cover about 15% of the area of the gold surface. This means that in the first approximation the second peak position (1.8 mg/cm^2) corresponds to a depth of about 1.1 μm [1]. This value fits well with the results obtained by the SEM/XEM method, presented in Fig. 1b (the gold layer thickness is 1.2 μm). This leads us to conclude that the second peak in the oxygen distribution plot (Fig. 7) corresponds to the gold-tungsten boundary and can be ascribed to the tungsten oxidation process.

It should be noted that in the centre of the irradiation zone the total amount of oxygen collected in the gold has increased more than 20 times in comparison to the non-irradiated wire. Moreover, the maximum value of the oxygen concentration increased up to 10 times, achieving a very high value of 1×10^{22} at/cm^3.

The concentration of oxygen measured near the gas outlet end of the wire is larger than what is measured near the gas inlet end. This is a good match with the results obtained by the SEM/XEM analysis. Evidently, the aging phenomenon described in Section 3.2 can be explained by the presence of oxygen in the aging processes at high-accumulated doses. Taking into account all these results, we propose a new mechanism for the anode wire aging, described in the next section.

3. Anode swelling – a new mechanism of anode wire aging

As mentioned above, the gas avalanche causes a plasma environment in which different types of active radicals are created. An analysis of the wire swelling phenomena, including data obtained earlier [2, 3] and the data presented above, leads us to propose a new mechanism for the anode wire aging. We attempt to describe this phenomenon in general terms and have no illusion that this process is entirely understood. Many aspects of the process are appropriate for later, more careful study. Our goal is to show the interconnection between the main factors that appear to cause the anode wire swelling and aging. The mechanism of wire aging development can be considered as three sequential stages.

3.1. Stage #1. Production of oxygen and others active chemical radicals in the gas avalanche

The wire aging can be an extremely complex chemical process. To obtain a general picture of the wire aging, it is necessary to identify the dominant processes occurring in gas avalanches, which result in the production of active chemical species (radicals, ions, *etc*). The avalanche environment is a plasma of ions and neutral radicals, and thus the wire aging process should be studied in the framework of plasma chemistry. We suppose that the most important plasma-chemical reactions for our gas mixture and their corresponding active radicals are as follows [6]:

$$e^- + CO_2 \rightarrow CO^\bullet + O^\bullet + e^-; \tag{2}$$
$$\hookrightarrow CO^\bullet + O^-; \tag{3}$$
$$\hookrightarrow CO^- + O^\bullet; \tag{4}$$
$$\hookrightarrow C^\bullet + 2O^\bullet + e^-; \tag{5}$$
$$\hookrightarrow C^\bullet + O^\bullet + O^-; \tag{6}$$
$$e^- + CO_2 \rightarrow CO^+ + O^- + e^-; \tag{7}$$
$$O^\bullet + O^- \rightarrow O_2^-; \quad O^\bullet + O_2^- \rightarrow O_3^-; \tag{8}$$
$$e^- + CF_4 \rightarrow CF_3^\bullet + F^-; \tag{9}$$
$$e^- + CF_4 \rightarrow CF_3^- + F^\bullet; \tag{10}$$
$$e^- + CF_4 \rightarrow CF_3^\bullet + F^\bullet + e^-; \tag{11}$$
$$\hookrightarrow CF_2^{\bullet\bullet} + 2F^\bullet + e^-. \tag{12}$$

Electrons created from the ionization of the gas move toward the anode wire in the intense electric field and gain sufficient energy to break the chemical bonds of the gas molecules. Thus, oxygen ions and radicals are produced due to the dissociation of CO_2 (dissociation energy E_d = 5.5 eV) around the anode wire. Reaction (7) is relatively unlikely to occur since its dissociation energy is much higher than that of the other reactions. The dissociation of CF_4 produces many different active species as well. Negative ions move to the anode surface under the influence of the electric field, are then neutralized there, but can still remain as chemically active neutral radicals. The remaining radicals can react with other species already existing in the avalanche plasma and also with new compounds produced in the avalanche plasma from a series of reactions. These reactions can involve the anode material, including the gold. Some possible chemical reactions are suggested later in sections 3.2 and 3.3: reactions (13)−(17).

An additional source of oxygen or oxygen-containing molecules (for instance, water vapour has E_d = 5.2 eV) comes from the diffusion of air and water vapour through the plastic wall of the straw tube [7].

The intensity of the ion and radical production depends on the gas composition, the detector irradiation rate, the electric field strength and the gas gain.

3.2. Stage #2. Oxygen penetration through the gold layer of the anode wire

The experimental data presented above (see Section 3, Figs. 2−5) lead us to conclude that defects in the gold layer are the main path for oxygen transportation to the tungsten. The defect creation scheme in the gold coating of the wire is shown in Ref. [1].

All defects can be differentiated into two groups:

- imperfections created in the gold coating during the wire manufacturing;
- damages created by the aging processes.

[6] M.Capeans *et al.*, Nucl. Instr. Meth. **A337**, 122 (1993);
L.G.Christophorou *et al.*, Nucl. Instr. Meth. **163**, 141 (1979);
I.C.Plumb and K.R.Ryan, Plasma Chem. Plasma Process **6**, 205 (1986).

[7] J.Wise, Plasma Chemistry in a Wire Chamber (M.S.Thesis), Report LBL-29033, 1990.

3.2.1. Imperfections created in the gold coating due to the wire manufacturing process

Gold is a crystal but not necessarily a mono-crystal. The gold coating has a crystalline structure, and the quality of the gold coating depends critically on the technology used in the wire manufacturing. The two technologies most often used are:

a) A tungsten wire is passed through a gold melt. This provides a well-bonded and uniform coating of the wire.

b) The gold is put on the tungsten wire using a method of chemical (galvanic) deposition. This method provides a fragile coating that has both a poorer structural quality and a higher permeability than the other process.

In both processes, the gold crystallite dimensions determine the gold film permeability. In the first case, it is ≤ 100 Å, and in the second case it is 100−1000 Å. It is necessary to point out a few factors directly affecting the quality of the gold coating during the wire manufacturing. Usually, the surface of the tungsten wire to be coated is rough and may contain implanted microparticles and oxides. Also, the adhesive of the gold to a tungsten surface is not very good. All of these factors result in the gold condensing as a crystallite structure only on separated areas of the tungsten surface, giving the coating an "island-like" character [8]. The gold crystals grow with different rates on the different crystal faces. Next, the growing elements of the crystallite structure mechanically join in a rough agglomerated film. In this case, the partial coalescence of the different crystallite shapes and orientations is possible. It results in the appearances of both open and closed imperfections, whose dimensions directly depend on the technology used for the gold coating.

3.2.2. Damages caused by the aging processes

Initial imperfections in the gold crystallite structure, which can increase and develop under the influence of sustained irradiation and etching of the gold, can provide favourable conditions for active oxygen with broken bounds, and even for more complicated chemical radicals, to penetrate into the tungsten.

Irradiation. Particle irradiation of metallic films (like the gold layer, for instance) provokes the creation of pores. An intense irradiation produces additional point defects in the gold coating, which intensify the process of gas accumulation and concentration in the local points of gold. This can result in the swelling of the gold coating.

Gold etching. In the case of a $Xe/CO_2/CF_2$ gas mixture, a chemical etching process may increase the permeability of the gold coating. The etching strongly attacks defects in the gold coating and results in their extension. It should be noted that the etching is a dangerous process which can open a direct path for the active oxygen to the tungsten surface of the wire. Reactions that could cause some etching on the gold surface are shown below. Special interest for our gas mixture are two chemical agents which determine possible gold etching: fluorine and xenon-fluorine XeF_n (n = 2, 4, 6) compounds.

Fluorine can slowly react [9] directly with the gold surface and provide direct fluorination of gold at 350°C. As will be discussed below, in the case of gas discharge a reaction is occurs at the room temperature:

$$2Au + 3F_2 \rightarrow 2AuF_3. \qquad (13)$$

It should be noted that such types of reactions involve molecular fluorine (F_2) which is not a component of our gas mixture. However, this does not prevent these reactions from occurring in our aging tests, since (F_2) will be dissociated in the avalanche. According to the literature [9], the reaction $F_2 \leftrightarrow 2F^\bullet$ required a temperature of about 800°C, or an electrical discharge at the room temperature. This is due to the fact that the F-F bond is very weak (E_d = 1.6 eV) and is easily broken in a avalanche, where the energy distribution of electrons is expected to be in the 1−10 eV range. So, the resulting radical, $F^\bullet$**,** is formed easily in our gas mixture and is very reactive.

---

8 S.P.Kukushkin and A.V.Osipov, Uspekhi Fiz. Nauk **168**, 1083 (1998).
J.E.Geguzin and Yu.S.Kaganovski, *Diffraction processes on crystal surfaces,* Energoizdat, Moscow, 1984.

9 R.A.Lidin, V.A.Molochko, and L.L.Andreeva, *Chemical properties of inorganic compounds,* Khimiya, Moscow, 1998.

It is well known that the *xenon-fluorine compounds*, XeF_n (n = 2, 4, 6), can readily appear in a gas discharge. The synthesis of XeF_2 using a high voltage discharge in mixtures of xenon and CF_4 is routinely successful. The mass spectrum showed conclusively that the crystals were the expected XeF_2. Peaks corresponding to XeF_2^+, XeF^+, Xe^+ and Xe^{++} were observed, having the correct isotopic distribution. At room temperature, XeF_n compounds are in a solid phase. Their densities and melting points are presented in Table.

Table

Compounds	Density of compounds	Melting points
XeF_2	3.13 g/cm^3	+ 129°C
XeF_4	3.03 g/cm^3	+ 117°C
XeF_6	3.41 g/cm^3	+ 49.5°C

These compounds are strong oxidizers and may interact with the gold causing the etching. Some possible chemical reaction chain is presented in (14).

Gas absorption. The phenomenon of gas absorption by the gold coating takes place both during the wire production procedure and in the interaction with the avalanche plasma. The gas, including oxygen, is absorbed by the outer layer of the gold and diffuses inside. The amount of absorbed oxygen depends on the temperature and the oxygen solubility in the gold, the irradiation intensity and the gas gain. It is important to note that an additional noticeable source of oxygen ions comes from the limited streamer mode, since the total charge produced per streamer may be a hundred times larger than that of a proportional pulse. This mode exists under our working conditions [5]. This phenomenon can be an additional source of damage to the gold coating of the wire.

$$\begin{aligned} &Xe + 2F^{\bullet} \rightarrow XeF_2; \\ &\qquad\qquad \downarrow \\ &\qquad Au + XeF_2 \rightarrow AuF_3 + Xe. \quad (14) \end{aligned}$$

3.3. Stage #3. Anode wire swelling

The comparison of the wire swelling (Fig. 1) and the oxygen concentration (Fig. 6) distributions along the wire leads us to the conclusion that the wire swelling might be caused by the chemical interaction of oxygen with the tungsten. This seems reasonable if we take into account the XEM spectra results (Fig. 1b) which confirm that both oxygen and tungsten are detected, indicating an oxidized tungsten surface. This process results, for instance, in the production of WO_3, whose density (7.3 g/cm^3) is 2.5 times less than that of tungsten (19.3 g/cm^3). This causes an increase in the wire volume, *i.e.* the wire swells.

Our model supposes that the tungsten oxide grows first in the point defects of the gold coating and exerts sufficient force to breach the gold in some local points. This point of view is confirmed by the data presented in Figs.1, 3 and 8. As one can see, pitting corrosion (see Fig. 8a) and damage to the gold coating develop along the grooves caused by the drawing die. It is also possible to see the gold layer splitting due to forces applied from within (Fig. 8b).

Hence, the wire swells due to the oxidation of the tungsten. As a consequence, the forces applied from within the wire break the gold coating. This is the main difference between our described mechanism and the well known polymerization mechanism of aging. A peculiar feature of the destruction of the coating

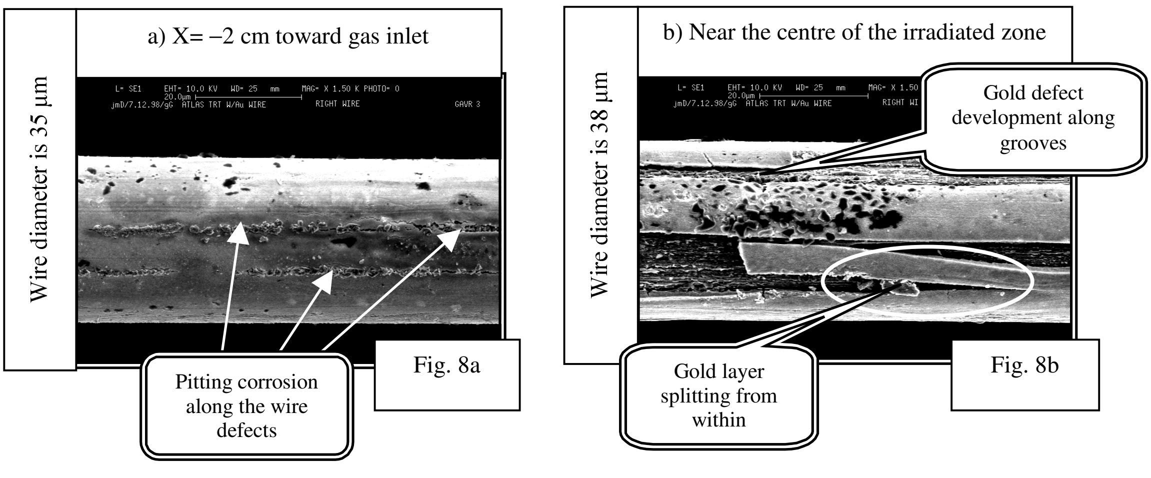

Fig. 8. Pictures showing the development of the local defects in the goal layer at two different points along the wire. The scale (20 μm) is indicated by the white line in the upper part of these figures

is its initial development along the tungsten wire. It takes place in the grooves along the wire caused by the drawing die used for the tungsten wire manufacturing, *etc.* As a result, the increase in the wire diameter is followed by deep cracks running along the wire, which stimulate the aging process. The forces affecting the gold coating are so strong that the film is disrupted. Fig. 1 shows the final stage of the anode wire swelling process, while Fig. 9 presents the schematic mechanism of this process.

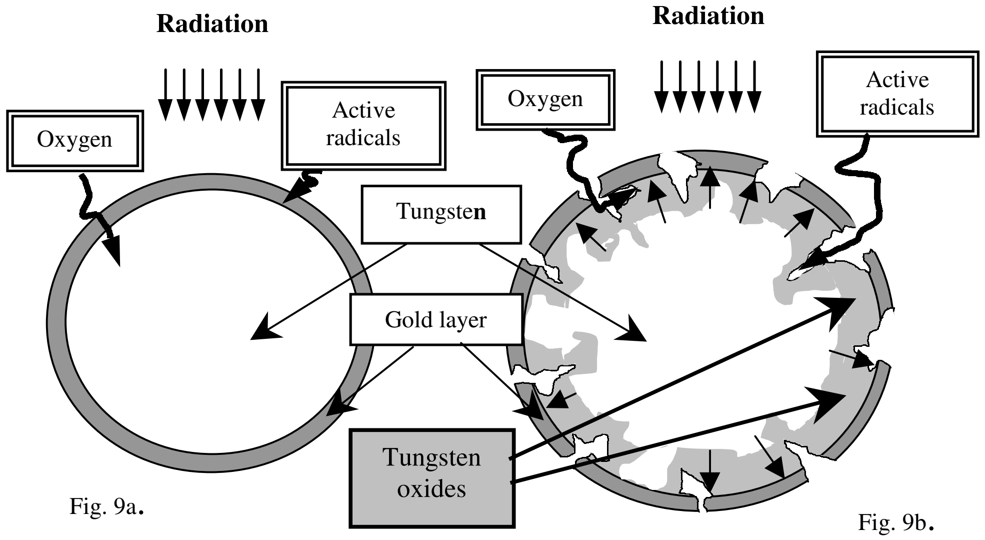

Fig. 9. The mechanism for the anode swelling effect. A schematic view of an anode wire cross section is shown before (Fig. 9a) and after (Fig. 9b) irradiation

Oxygen and other aggressive radicals penetrate through the already opened cracks in the gold layer and react directly with the tungsten. As a result, the oxidation of the tungsten occurs.

More complicated chemical products can also be created in the reaction between the different gas radicals and the tungsten. These species can be produced in non-volatile (↓) or volatile (↑) forms. Some possible products [9] are shown below:

$$W + F_2/O_2 \rightarrow WOF_4\downarrow; \quad (15)$$
$$W + 3F_2 \rightarrow WF_6\uparrow; \quad (16)$$
$$2WO_3 + 6F_2 \rightarrow 2WF_6\uparrow + 3O_2 . \quad (17)$$

WF_6, for instance, is already in a volatile form at the room temperature. Its ablation from the tungsten might cause additional damage to the gold surface of the wire inside the irradiation zone.

Some substances (deposits) could be created due to a corrosive pitting between the active oxygen (and other radicals), dispersed by the gas flow, and the wire material. Such deposits should be distributed along the wire but asymmetrically with respect to the gas flow direction. The deposition rate is determined by the intensity of the ion and radical creation and by the gas flow rate.

4. Conclusion

1. Aging studies of straw-tubes, used with a 70% Xe + 10% CO_2 + 20% CF_4 gas mixture, have been performed. It has been shown that under a high accumulated dose (about 9 C/cm) and a dose rate corresponding to 1.7 μA/cm, a new aging mechanism of the anode wire – the swelling of the wire – was observed. The results of SEM/XEM examination of the wire surface have shown that in the centre of the irradiated zone the gold coating is broken and the wire diameter increased from 35 μm to 42 μm (20%). The intensive peak of oxygen has been observed on the open tungsten surface among the pieces of the gold coating.

2. In order to establish the penetration of light elements into the wire gold coating, Nuclear Reaction Analyses (NRA) was applied. To investigate the kinetics of oxygen transport inside the gold, the $^{16}O(d,p)^{17}O$ reaction was used. It has been shown that the average concentration of oxygen at the beginning of irradiation is about 1×10^{21} at/cm^3. The total amount of oxygen collected in the wire increased more than 20 times in comparison with the non-irradiated wire after an accumulation of 9 C/cm in the centre of the irradiation zone. Moreover, the maximum value of oxygen concentration increased by up to 10 times and achieved a very high value of 1×10^{22} at/cm^3.

The NRA reliably confirms both the important role of oxygen in the anode wire swelling mechanism and that the kinetics of the oxygen transportation into the depth of the gold coating really exists.

3. Using NRA in combination with SEM/XEM, we have obtained much more precise and complete information about the anode wire swelling phenomenon. Taking into account these data, a mechanism of anode wire aging is proposed, in which we distinguished three sequential stages.

3.1. The oxygen and other active radicals are created in the gas avalanche. Defects in the gold layer are the main path for the active oxygen transportation to the tungsten. These defects are created by the gold coating technology and, in addition, by the chemical etching of the gold by species produced in the gas avalanche. Eventually, the etching process leads to the growth of the cracks and the volume porosity of the gold coating.

3.2. The oxygen penetrates through the pores and cracks of the gold layer and, as we assume, oxidizes the tungsten.

3.3. Finally, this causes the swelling of the tungsten in the wire and, as a consequence, forces produced within the wire break the gold coating. Aggressive radicals, including active oxygen, penetrate through the already opened cracks in the gold layer and react directly with the tungsten. As a result, the swelling of the tungsten occurs.

4. It has been found that the atomic oxygen plays a very important role in this anode wire aging process. We believe that measurements performed using NRA of the oxygen concentration and the depth of its penetration into the gold coating after irradiation provide an excellent method to compare the aging resistance of different wires.

5. The presence of xenon in the gas causes additional pathways for active chemical radical creation. Xenon and xenon fluorides amplify the etching process and provide an easy path for the oxygen to reach the tungsten.

References

[1] T.Ferguson, G.Gavrilov, A.Krivchitch, E.Kuznetsova, and L.Schipunov, Preprint PNPI-2331, Gatchina, 1999.

[2] T.Ferguson, G.Gavrilov, A.Egorov, A.Krivchitch, E.Kuznetsova, V.Lebedev, and L.Schipunov, Nucl. Instr. Meth. **A483**, 698 (2002).

[3] G.Gavrilov, A.Krivchitch, E.Lobachev, and L.Schipunov, Preprint PNPI-2212, Gatchina, 1997.

[4] G.Gavrilov, A.Krivchitch, V.Lebedev, and V.Smolin, Preprint PNPI-2227, Gatchina, 1998.

[5] T.Ferguson *et al.,* Aging Investigation of CMS EMU Prototype Chambers, CMS External Note 1999/011 (04.02.1999).

[6] G.Gavrilov, A.Krivchitch, A.Kuznetsova, E.Lobachev, and L.Schipunov, Preprint PNPI-2328, Gatchina, 1999.